한국정밀공학회지 제16권 제5호 (1999년 5월)
Journal of the Korean Society of Precision Engineering Vol. 16, No. 5, May 1999.

공중파용 비선형적 초음파 감지센서의 설계를 위한 수치 해석

이양섭*

Numerical Analysis for Designing Nonlinearly Ultrasonic Proximity Sensors in Air

Yang Sub Lee*

ABSTRACT

이상적인 초음파 물체 감지 센서는 감지거리가 길고, 고해상도와 작은 크기이어야 한다. 그러나 현재 공기 중에 사용되고 있는 선형 초음파센서로는 공기의 높은 음흡수 때문에 이 세 가지 조건을 동시에 만족하기는 어렵다. 본 논문은 서로 다른 주파수성분의 두 음파의 비선형 상호작용으로 생성되는 두 주파수 차이에 상당하는 주파수의 음파를 이용한 물체감지 비선형적 초음파 감지센서에 관한 연구이다. 링-디스크 두 요소로 구성된 비선형적 초음파센서에 의해 형성되는 음장을 예측할 수 있는 컴퓨터 프로그램을 개발하였으며, 이 프로그램을 이용하여 비선형적 초음파센서의 최적 형태와 주파수를 결정하고, 선형 초음파센서와 세 조건 측면에서 비교 검토하였다. 비교 결과 비선형적 초음파센서가 해상도측면에서 유리하고, 75 dB이하의 초음파 소음환경에서 사용할 때 감지거리면에서 유리하다.

Key Words: Ultrasonic (초음파), Sensor (센서), Resolution (해상도), Detecting distance (감지거리), Difference frequency (차주파수), Linearity (선형), Nonlinearity (비선형), Program (프로그램)

1. Introduction

Ultrasonic proximity sensors have been used as an alternative to optical systems for measuring the distance to objects with high degree of accuracy. Advantages offered by ultrasonic versus optical proximity sensors are their simplicity of operation, lower cost, and their ability to function in environments which are optically opaque. However, the high absorption of sound by air at high ultrasonic frequencies makes achieving long range and high resolution with a small transducer element difficult to accomplish with conventional designs[1,2].

In this paper we consider a parametric array[3]

* 계명대학교 자동차공학부

(described below) as an alternative to conventional ultrasonic sensor design for proximity sensing. Parametric arrays have been used successfully in underwater sonar application where absorption poses problems for long range detection.

A parametric array is formed by two collinear, finite amplitude sound beams of different frequency which interact nonlinearly to produce a narrow beam of difference frequency sound. The interaction of the two primary beams also generates sum frequency and second harmonic components, as well as higher-order intermodulation components. However, the difference frequency component is of great interest because, having a potentially much lower frequency than the primary, sum frequency, and second harmonic waves, it is less affected by absorption and thus propagates further.

Conventional ultrasonic sensors whose radiated sound fields are governed by linear acoustical theory are hereafter referred to as linear sensors. Ultrasonic sensors whose sound fields result from the nonlinear process of parametric interaction are referred to as nonlinearly ultrasonic sensors or parametric sensors.

To avoid the undesirable nonlinear mixing[4] in the transducer, we consider a transducer consisting of only two elements, a circular (disk) source encircled by a second, doughnut-shaped (ring) source for generating the primary beams in parametric array. The disk and the ring are driven at different frequencies.

In this paper, we compare a linear sensor[2] having a 1 cm radius and 200 kHz operating frequency with comparable parametric sensors in terms of high resolution, long range, and small size by applying appropriate linear and nonlinear acoustical theories. A linear sensor having the above parameters has been used to acoustically detect an object in air. For the parametric sensors we choose the outer radius and the average primary frequency to match those of the linear circular sensor, i. e., 1 cm and 200 kHz, respectively. The nonlinearly generated difference frequencies which are considered are 50 kHz and 80 kHz, respectively.

Optimization of design parameters, such as source geometry and operating frequencies, for efficient generation of the difference frequency sound is also carried out on the basis of both linear and nonlinear acoustic theories.

2. Theory

A parabolic nonlinear wave equation which provides an excellent model for the combined effects of nonlinearity, diffraction, and dissipation in directive sound beams is the KZK (Khokhlov-Zabolotska-Kuznetsov) equation[5,6]. The KZK equation can be written:

$$\frac{\partial^2 p}{\partial z\,\partial \tau}-\frac{c_0}{2}\nabla_\perp^2 p-\frac{b}{2\rho_0 c_0^3}\frac{\partial^3 p}{\partial \tau^3}=\frac{\beta}{2\rho_0 c_0^3}\frac{\partial^2 p^2}{\partial \tau^2} \qquad (1)$$

where $p(x, y, z, \tau)$ is the acoustic pressure, $\tau = t - z/c_o$ retarded time, c_o the small signal sound speed, ρ_0 ambient density of the fluid, b the sound diffusivity of a thermoviscous medium, $\nabla_\perp^2 = \partial^2/\partial x^2 + \partial^2/\partial y^2$ the transverse Laplacian operator, and $\beta = (\gamma+1)/2$ is the coefficient of nonlinearity, where γ is the ratio of specific heats. The second term and the third term on the left-hand side of Eq. (1) account for diffraction and absorption, respectively, and the term on the right-hand side for nonlinearity. Equation (1) was first obtained by Kuznetsov[5,6]. Although Eq. (1) is written for a thermovicous fluid, it is valid for a relaxing fluid, i.e., air, provided the absorption coefficient (α) is proportional to frequency (f) squared over the frequency range of interest. For the frequencies considered in this paper, the f^2 dependence holds reasonably well. Unless otherwise stated, all absorption coefficients in this paper are calculated using the relation $\alpha = 2.0\times10^{-11}\times f^2$, obtained from Ref. 7 for a temperature of 20° C and a pressure of 1 atmosphere. Within the approximation inherent in the derivation of the KZK equation, it is consistent to use the linear planar

wave impedance relation $p=\rho_0 c_0 u$, where u is the z component of the particle velocity.

Two well-developed quasilinear solutions of Eq.(1) are available for the difference frequency sound beams. One is a quasilinear integral solution obtained by the Tjotta and Garrett[8,9,10], and another is a modified Gaussian beam solution[11,12].

The quasilinear integral solution for garrett[8] for the difference frequency component which is obtained for weak nonlinearity is applicable to the case of a source with axisymmetric but otherwise arbitrary on-source distribution. However, since the quasilinear integral solution of Garrett et al.[8] for the difference frequency component involves a quadruple integration which requires considerable computation time, the integral solution was not used in this paper.

The modified Gaussian beam solution of Eq. (1) for the difference frequency sound for a circular piston source is obtained by approximating a uniform circular piston source with a Gaussian source[11,12]. Hamilton and Fenlon[12] showed that the modified Gaussian solution for a circular piston is in good agreement with experimental data for the difference frequency obtained in water along the axis and within 5 degrees off the axis of the parametric array. Since the source considered in this paper for generating the difference frequency sound consists of a disk piston and a ring piston rather than a single disk, the modified Gaussian beam solution is not applicable.

In this paper, we have instead developed quasilinear finite difference numerical solutions of the KZK equation for calculating the sound fields from acoustic sensors. The finite difference solution requires considerably less computation time than the integral solution of Garrett et al.[8].

We now introduce a reference frequency ω_1 and effective on-source pressure amplitude p_{01}. Equation (1) can then be written in terms of nondimensional variables as follows:

$$(4\frac{\partial^2}{\partial\tau_s\partial\sigma}-\nabla_{\perp}^2-4\alpha_1 z_o\frac{\partial^3}{\partial\tau_s^3})P=2\frac{1}{\sigma_D}\frac{\partial^2}{\partial\tau_s^2}P^2. \tag{2}$$

Here $\tau_s=\omega_1\tau$, $\sigma=z/z_0$, $\xi=r/a$, $P=p/p_{01}$, $\nabla_{\perp}^2$ is the nondimensional transverse Laplace operator with respect to ξ, $r=(x,y)$ is a position vector, and $z_o=k_1a^2/2$ is a Rayleigh distance, where a is a characteristic length transverse to the source (a is usually the source radius). We also introduce $\sigma_D=l_d/z_o$, where $l_d=c_0/\beta\varepsilon_1\omega_1$ is the shock formation distance of a plane wave, $\alpha_1=b\omega_1^2/2\rho_0c_0^3$, and $\varepsilon_1=p_{01}/\rho_0c_0^2$ is a Mach number. The notation is similar to that used by Aanonsen et al.[13].

It is useful for efficient numerical calculations to write Eq. (2) in terms of the new variables

$$T=(1+\sigma)P,\quad v=\frac{\xi}{(1+\sigma)},\quad \tau_q=\tau_s-\frac{\xi^2}{(1+\sigma)}, \tag{3}$$

where $\xi=|\xi|=|r|/a$. In terms of $T(\sigma, v, \tau_q)$, Eq. (2) becomes

$$(4(1+\sigma)^2\frac{\partial^2}{\partial\tau_q\partial\sigma}-\nabla_v^2-4\alpha_1 z_o(1+\sigma)^2\frac{\partial^3}{\partial\tau_q^3})T=2\frac{(1+\sigma)}{\sigma_D}\frac{\partial^2}{\partial\tau_q^2}T^2, \tag{4}$$

where ∇_v^2 is the two-dimensional Laplace operator with respect to the variable v. With $(1+\sigma)$ replaced by σ, Eq. (4) is formally equivalent to Eq. (8) in Ref. 14.

The linearized version of Eq. (4), which we use for the primary waves, is

$$(4(1+\sigma)^2\frac{\partial^2}{\partial\tau_q\partial\sigma}-\nabla_v^2-4\alpha_1 z_o(1+\sigma)^2\frac{\partial^3}{\partial\tau_q^3})T_i=0, \tag{5}$$

where T_i is the transformed field variable for the i th primary wave ($i=1,2$). A solution of Eq. (5) may be sought in the form

$$T_i=G_i\sin(\Omega_i\tau_q)+H_i\cos(\Omega_i\tau_q), \tag{6}$$

where $\Omega_i = \omega_i/\omega_1$ is a dimensionless frequency ratio, and ω_1 and ω_2 are the two source frequencies. Substituting Eq. (6) into Eq. (5) and identifying the terms in $\sin(\Omega_i\tau_q)$ and $\cos(\Omega_i\tau_q)$, we obtain the following set of coupled differential equations for the components $G_i(\sigma, v)$, and $H_i(\sigma, v)$:

$$\frac{\partial G_i}{\partial \sigma} = -\Omega_i^2 \alpha_1 z_o G_i + \frac{1}{4\Omega_i(1+\sigma)^2} \nabla_v^2 H_i ,$$
$$\frac{\partial H_i}{\partial \sigma} = -\Omega_i^2 \alpha_1 z_o H_i - \frac{1}{4\Omega_i(1+\sigma)^2} \nabla_v^2 G_i . \tag{7}$$

The inhomogeneous form of Eq. (4) for the second harmonic, sum, and difference frequency waves is obtained by substituting $(T_1+T_2)^2$ for T^2 in the right-hand side of Eq. (4)

$$(4(1+\sigma)^2 \frac{\partial^2}{\partial\tau_q \partial\sigma} - \nabla_v^2 - 4\alpha_1 z_o (1+\sigma)^2 \frac{\partial^3}{\partial\tau_q^3}) T$$
$$= 2\frac{(1+\sigma)}{\sigma_D} \frac{\partial^2}{\partial\tau_q^2} [G_1 \sin(\Omega_1\tau_q) + H_1 \cos(\Omega_1\tau_q)$$
$$+ G_2 \sin(\Omega_2\tau_q) + H_2 \cos(\Omega_2\tau_q)]^2, \tag{8}$$

where

$$[G_1 \sin(\Omega_1\tau_q) + H_1 \cos(\Omega_1\tau_q) + G_2 \sin(\Omega_2\tau_q)$$
$$+ H_2 \cos(\Omega_2\tau_q)]^2 = \frac{1}{2}(G_1^2 + G_2^2 + H_1^2 + H_2^2)$$
$$+ G_1 H_1 \sin(2\Omega_1\tau_q) + \frac{1}{2}(H_1^2 - G_1^2)\cos(2\Omega_1\tau_q)$$
$$+ G_2 H_2 \sin(2\Omega_2\tau_q) + \frac{1}{2}(H_2^2 - G_2^2)\cos(2\Omega_2\tau_q)$$
$$+ (G_1 G_2 + H_1 H_2)\cos(\Omega_-\tau_q) + (G_1 H_2 - H_1 G_2)$$
$$\sin(\Omega_-\tau_q) + (G_1 H_2 + H_1 G_2)\sin(\Omega_+\tau_q)$$
$$+ (H_1 H_2 - G_1 G_2)\cos(\Omega_+\tau_q), \tag{9}$$

and where $\Omega_- = \Omega_1 - \Omega_2$ and $\Omega_+ = \Omega_1 + \Omega_2$. The following inhomogeneous equation for the difference frequency sound field is obtained by substituting for T_- in the left-hand side and retaining only the terms containing Ω_- on the right-hand side of Eq. (8):

$$(4(1+\sigma)^2 \frac{\partial^2}{\partial\tau_q \partial\sigma} - \nabla_v^2 - 4\alpha_1 z_o (1+\sigma)^2 \frac{\partial^3}{\partial\tau_q^3}) T_-$$
$$= 2\frac{(1+\sigma)}{\sigma_D} \frac{\partial^2}{\partial\tau_q^2} [G_1 G_2 + H_1 H_2)\cos(\Omega_-\tau_q)$$
$$+ (G_1 H_2 - H_1 G_2)\sin(\Omega_-\tau_q)] \tag{10}$$

If a solution of Eq. (10) is sought in the form

$$T_- = G_- \sin(\Omega_-\tau_q) + H_- \cos(\Omega_-\tau_q),$$

then the following set of coupled equations for the components $G_-(\sigma, v)$ and $H_-(\sigma, v)$ is obtained by separating Eq. (10) with respect to the coefficients of $\sin(\Omega_-\tau_q)$ and $\cos(\Omega_-\tau_q)$

$$\frac{\partial G_-}{\partial \sigma} = -\Omega^2 \alpha_1 z_o G_- + \frac{1}{4\Omega_-(1+\sigma)^2} \nabla_v^2 H_-$$
$$- \frac{\Omega_-}{2\sigma_D(1+\sigma)}(G_1 G_2 + H_1 H_2),$$
$$\frac{\partial H_-}{\partial \sigma} = -\Omega_-^2 \alpha_1 z_o H_- - \frac{1}{4\Omega_-(1+\sigma)^2} \nabla_v^2 G_-$$
$$+ \frac{\Omega_-}{2\sigma_D(1+\sigma)}(G_1 H_2 - H_1 G_2). \tag{11}$$

We now consider the boundary conditions. For an axisymmetric source which oscillates sinusoidally with amplitude $F_i(\xi)$, the boundary conditions at $\sigma = 0$ become

$$F_i(\xi)\sin(\Omega_i\tau_s) = F_i(v)\sin\Omega_i(\tau_q + v^2)$$
$$= F_i(v)[\cos(\Omega_i v^2)\sin(\Omega_i\tau_q) + \sin(\Omega_i v^2)\cos(\Omega_i\tau_q)]$$

where $v = |\boldsymbol{v}| = \xi$ at $\sigma = 0$. We thus obtain for the boundary conditions on G_i and H_i at $\sigma = 0$:

$$G_i = F_i(v)\cos(\Omega_i v^2) \text{ and } H_i = F_i(v)\sin(\Omega_i v^2) \tag{12}$$

Equations (7) and (11) are stepwise integrated by an implicit backward finite difference method developed by Aanonsen[15]. Considerations of symmetry define the additional boundary condition at $v = 0$[15]. The region of numerical integration is also limited by specifying a maximum value (v_{max}) of v and setting the amplitude of the wave to zero when $v = v_{max}$. The value of v_{max} must be sufficiently large to avoid significant errors that are introduced by the imposed artificial boundary condition at $v = v_{max}$. Additional details about the numerical method and inherent errors associated with

our algorithm may be found in Refs. 14 and 15.

3. Comparisons with Existing Experimental Data

To this day, the results published by Bennett and Blackstock[4] for the difference frequency sound field are the most complete parametric array data in air. Bennett and Blackstock conducted experiments using a single circular source from which both primary beams were radiated uniformly with equal phase. The source had an effective radius a of 2.9 cm, and it was excited uniformly with effective on-source pressure amplitudes 10.5 Pa and 23.7 Pa at the frequencies 23.6 kHz and 18.6 kHz, respectively. They measured the propagation curves and beam patterns at a range of 2ft for the difference frequency sound field.

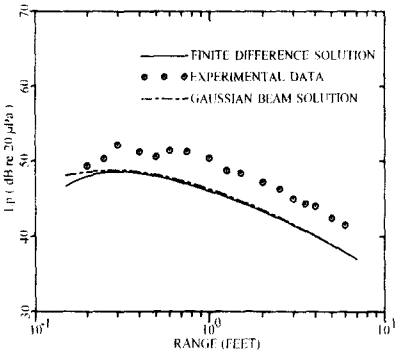

Fig. 1 Comparisons with existing experimental data

The propagation curves for the difference frequency sound obtained from both the modified Gaussian beam solution of Eq. (1) (with Eq. (A4) in Ref. 12) and the finite difference numerical solution of Eq. (1) (with the numerical method described in Section 2) for the above circular source are plotted in Fig. 1 for the difference frequency sound along with the corresponding experimental data by Bennett and Blackstock (which are excerpted from Ref. 4).

The two theoretical solutions agree well with each other, and there is an approximately 3.0 dB difference between both solutions and experimental data. Our results support the explanation for the 3dB difference given by Bennett and Blackstock[4] that the discrepancy might be due to experimental errors, such as errors in the three absolute amplitude measurements (one for each primary wave and one for the difference frequency component).

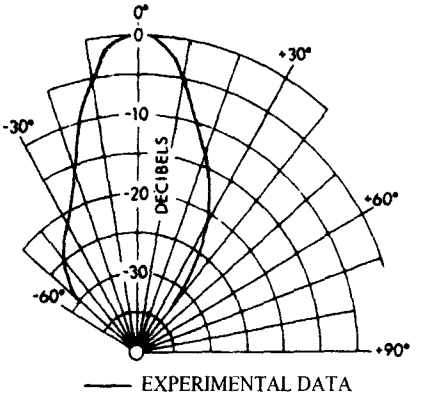

(a) Experimental beam pattern

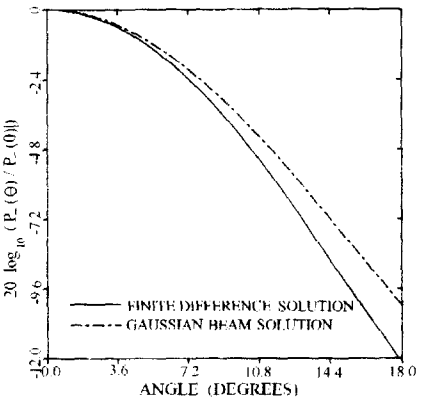

(b) Theoretical beam patterns

Fig. 2 Beam patterns

Experimental beam pattern at z=2 ft excerpted from Ref. 4 is shown in Fig. 2(a), and the theoretical beam patterns at a range of z=2 ft based on the Gaussian beam solution and finite difference

solution are presented in Fig. 2(b). Note that the abscissa in Fig. 2(b) for the theoretical beam patterns is the observation angle as measured along a line perpendicular to the z axis, while the experimental beam pattern of Fig. 2(a) was measured at points which are equidistant from the source. Examining Figs. 2(a) and 2(b), we see that the theoretical prediction obtained from the finite difference solution is in reasonable agreement with the corresponding measured data within the paraxial region. The Gaussian beam solution predicts a wider beam beyond approximately 5 degrees from the acoustic axis as in case of experiment in water of Ref. 8.

The quasilinear finite difference numerical solution can thus be considered to be a reliable solution to calculate the difference frequency sound field from a source with a weakly finite amplitude on-source level.

4. Optimization of Design Parameters

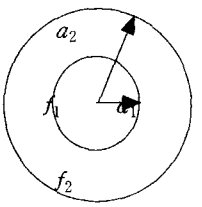

Fig. 3 Source configuration

The source which is used to produce the difference frequency sound field is composed of two elements, a circular (disk) source encircled in a second, doughnut-shaped (ring) source. The disk and the ring are excited with uniform velocity and uniform phase, while the former radiates at one of the primary frequencies, and the latter at the other frequency. The outer radius a_2 of the ring piston is fixed at 1cm, and the inner radius a_1 of the ring piston, i.e., the (outer) radius of the circular piston is a variable parameter. The variations of the inner radius a_1 are characterized by the dimensionless parameter $A = a_1 / a_2$ (See Fig. 3 for the configuration).

The quasilinear finite difference numerical solutions (which are obtained with the finite difference numerical method described in Section 2) are used in this paper to calculate the nonlinearly generated difference frequency sound field from the parametric (nonlinear) sensors of a disk and ring configuration. The operating frequencies of the source are 240 kHz and 160 kHz, and therefore the difference frequency is 80 kHz. Since f_1 denotes the frequency of the inner disk source and not the higher of the two primary frequencies, the difference frequency f_- is interpreted as the magnitude of $|f_1 - f_2|$. The average frequency is thus 200 kHz. The following values of constants are hereafter used in the computations: c_0=343 m/s, ρ_0=1.21 Kg/m^3 and γ= 1.4[4.7].

Figure 4 shows the normalized on-axis amplitude $|p_-|/p_0$ (in dB) of the difference frequency sound pressure for the sources with different values of A. Here, p_0 is the effective on-source sound pressure amplitude and $|p_-|$ the difference frequency sound pressure amplitude. In Fig. 4(a) the frequency of the circular piston is 240 kHz, and the frequency of the ring piston is 160 kHz. In Fig. 4(b), the frequencies are reversed. We observe that reversing the frequencies does not significantly affect the on-axis pressure amplitude of the difference frequency sound beyond 0.1 m, and the highest on-axis pressure is obtained in each case when A=0.6

The absorption length $L_A = (\alpha_1 + \alpha_2 - \alpha_-)^{-1}$ provides a reasonable estimate of the farfield region of the difference frequency sound field (see Ref. 3). Note that the L_A does not contain parameters related to source geometry. The absorption length for the nonlinear sensor is 65cm. Beam patterns of the difference frequency sound for sources with A=0.4 and A=0.7 with f_1=240 kHz (inner source) and f_2=160 kHz (outer source) are plotted at various

ranges (both less and greater than L_A) in Fig. 5.

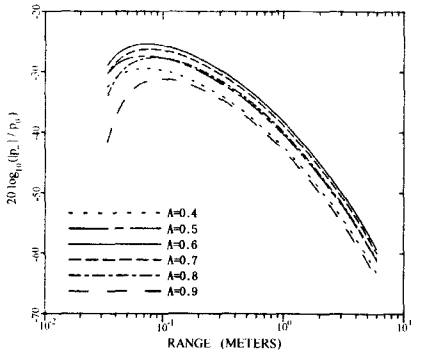

(a) f_1=240 kHz and f_2=160kHz

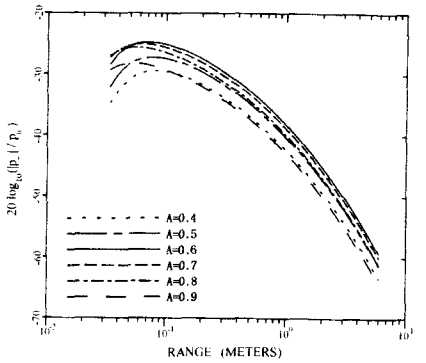

(b) f_1=160 kHz and f_2=240 kHz

Fig. 4 Normalized on-axis sound pressure amplitude of the difference frequency (f=80 kHz)

The abscissa for each beam pattern is the observation angle as measured along lines which are perpendicular to the acoustic axis. The directivity increases (i.e., the beam patterns becomes narrower) up to about 60cm, after which the directivity remains essentially constant. Since L_A=65 cm, the farfield of the parametric array evidently begins at approximately $z = L_A$.

Beam patterns of the difference frequency sound at a range of 1.5m (z=2.3 L_A) for sources with various values of A are plotted in Fig. 6. Again, note that the inner source radiates the higher frequency in Fig. 6(a), whereas the outer source radiates the higher frequency in Fig. 6(b). We see that the difference frequency beam patterns become slightly narrower at angles less than 5 degrees as the value of A increases, i.e., the narrowest beam patterns takes place when A=0.9, both before and after reversing the frequencies. Note that the beam patterns for f_1=160 kHz and f_2 =240 kHz are much narrower than those for f_1=240 kHz and f_2 =160 kHz. That is, narrower beams of the difference frequency sound are obtained when the outer ring is excited at the higher primary frequency.

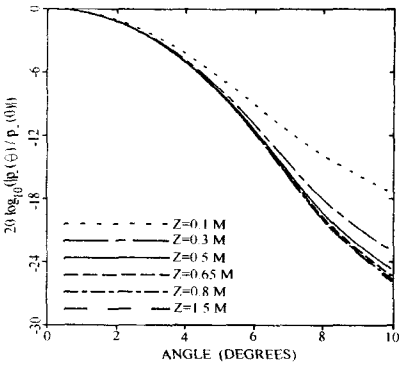

(a) A=0.4

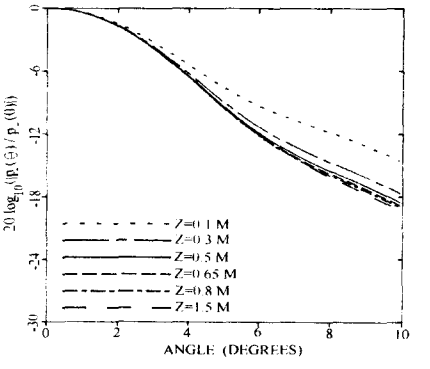

(b) A=0.7

Fig. 5 Beam patterns of the difference frequency sound (f=80 kHz) for sources with f_1=240 kHz and f_2=160 kHz

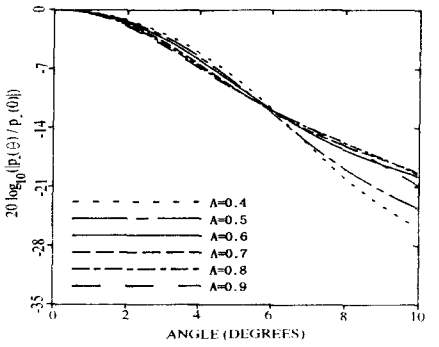

(a) f_1=240 kHz and f_2=160 kHz

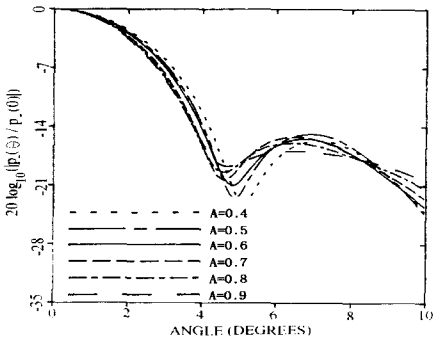

(b) f_1=160 kHz and f_2=240 kHz

Fig. 6 Beam patterns of the difference frequency sound (f_-=80 kHz) at a range of 1.5 m

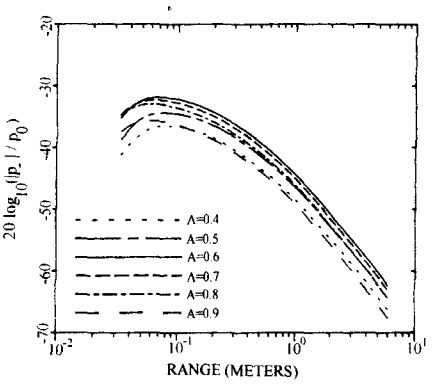

(a) f_1=175 kHz and f_2=225 kHz

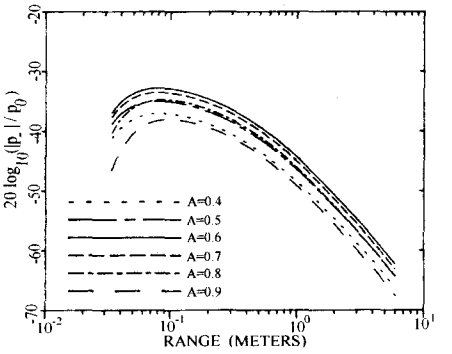

(b) f_1=225 kHz and f_2=175 kHz

Fig. 7 Normalized on-axis sound pressure amplitude of the difference frequency (f_-=50 kHz)

We now consider excitations of the source at the primary frequencies of 225 kHz and 275 kHz. The difference frequency is now 50 kHz, while the average frequency of the primaries is again 200 kHz. Figure 7 presents the normalized on-axis sound pressure amplitude $|p_-|/p_0$ (in dB) for cases where the higher primary frequency excites either the inner or outer source. We find again that switching the frequencies produces only a negligible change in the general trend, and the highest on-axis pressure occurs again with A=0.6, just as in case of the 80 kHz difference frequency.

The dependence of the corresponding beam patterns on A at a range of 1.5m is shown in Fig. 8. We see that the general trends are the same as in the case for f_-= 80 kHz. That is, the difference frequency beam pattern becomes narrower within the major lobe as the value of A increases, regardless of whether the higher primary frequency excites the inner or outer source. However, the beam patterns for f_1=175 kHz and f_2=225 kHz are much narrower than those for f_1=225 kHz and f_2=175 kHz.

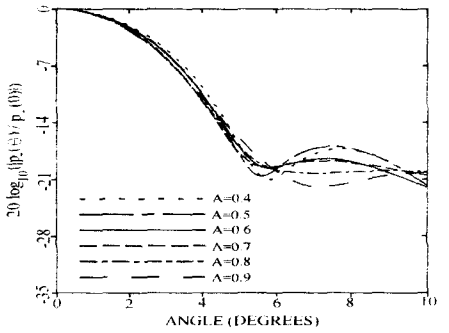

(a) f_1=175 kHz and f_2=225 kHz

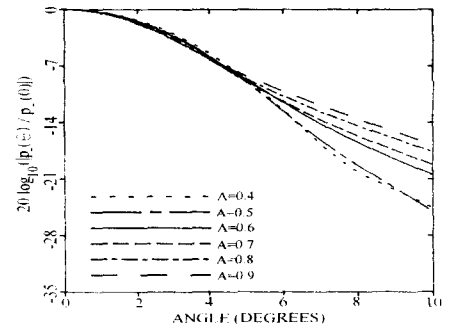

(b) f_1=225 kHz and f_2=175 kHz

Fig. 8 Beam patterns of the difference frequency sound (f=50 kHz) at a range of 1.5 m

We have found that the highest on-axis pressures for both 80 kHz and 50 kHz difference frequency are obtained when A=0.6. The next highest pressures on axis occur when A=0.7, in which case the on-axis pressures are approximately 0.5dB below those when A=0.6. Since this difference is negligible in view of inherent errors in the finite difference numerical solution, optimal value of A is considered to be between 0.6 and 0.7.

5. Comparisons

We shall compare two parametric (nonlinear) sensors with a linear sensor with a 1 cm radius and 200 kHz operating frequency which has been used for detecting the presence of an object in air. Both parametric sensors have an outer radius of 1 cm and a ratio of the inner to outer radius given by A=0.6. One parametric sensor is excited at frequencies f_1=160 kHz and f_2=240 kHz to generate a difference frequency of 80 kHz. The other is excited at frequencies f_1=175 kHz and f_2 =225 kHz to generate a difference frequency of 50 kHz. The average primary frequency in each case is 200 kHz. The on-source levels are the same for both the linear and parametric sensors. The decision to excite the ring source with the higher primary frequency was motivated by the results in Figs. 6 and 8, which demonstrate that narrower difference frequency beam patterns are obtained with this configuration.

Figure 9 show propagation curves for the linear and parametric sensors when the on-source levels are 130 dB (re 20 μPa). The on-source level of 130dB is almost the upper limit level up to which our quasilinear model (i.e., quasilnear solutions) are expected to be valid. Here the on-source level represents the value of $20\log_{10}[p_0/\sqrt{2}p_{ref}]$. The on-axis sound field for each parametric sensor is obtained using the quasilinear finite difference numerical solutions of the KZK equation, and the on-axis sound field for the linear sensor is also calculated from the finite difference solutions of the linear KZK equation (i.e., Eq. (5) for the primary wave) with the finite difference numerical method described in Section 2.

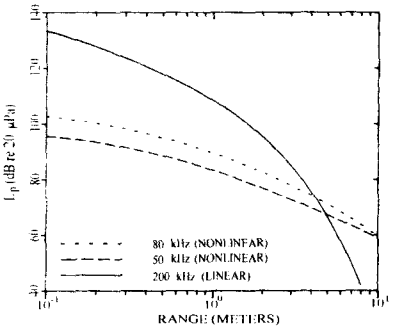

Fig. 9 Comparison of propagation curves for the linear and nonlinear sensors

If the target is assumed to be an ideal plane reflector normal to the acoustic axis, the range in Fig. 9 can be interpreted as the total distance, i.e., the round-trip distance from the source to the target. From Fig. 9 we see that the sound pressure levels of the parametric sensors exceed those of the linear sensor at levels below about 75 dB at the on-source sound pressure level of 130 dB.

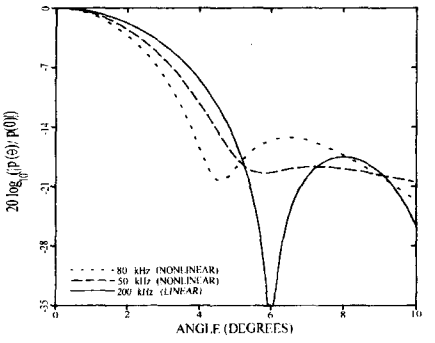

Fig. 10 Comparison of beam patterns for the linear and nonlinear sensors at a range of 1.5 m

Shown in Fig. 10 are the directivity patterns for the above linear and parametric (nonlinear) sensors at a range of 1.5m, which are calculated from the finite difference numerical solution of the linear KZK equation and the quasilinear finite difference numerical solutions of the KZK equation, respectively. The directivity pattern of the parametric sensor is narrower than that of the linear sensor.

6. Conclusions

We have considered a parametric sensor composed of two elements, a circular disk source embedded in a second ring source. The outer radius of the ring piston is fixed at 1 cm, and inner radius of the ring, i.e., the radius of the inner disk, is a variable parameter.

The optimal value of $A = a_1 / a_2$ (ratio of inner radius to outer radius of the source) for most efficient generation of a difference frequency sound field is considered to be between 0.6 and 0.7 for a disk and ring source configuration. Reversing the inner and outer frequencies does not significantly affect the on-axis sound field, but it does noticeably affect the beam patterns. In particular, when the ring piston is excited at the higher of the two primary frequencies, the main lobe in the difference frequency beam is narrower.

A parametric sensor having a ring-disk configuration with optimal relative frequencies and radii is compared with a linear sensor having a single disk configuration with a 1 cm radius and 200 kHz operating frequency. The comparison is made on the basis of long range, high resolution, and small size at the on-source levels of 130 dB.

Subject to the given design considerations, the parametric ultrasonic sensors, operating at primary frequencies having a mean of 200 kHz at on-source level of 130dB, offer advantage over conventional ultrasonic sensors when operated in air at the background noise level below 75dB at ultrasonic frequencies.

The quasilinear finite difference numerical solutions of the KZK equation which we have developed can be used for calculating the nonlinearly generated difference frequency sound fields from nonlinear acoustic sensors operating in other media as well as air and water, provided the absorption coefficient is proportional to frequency squared over the frequency range of interest.

References

1. R. Hickling and S. P. Marin, "The use of ultrasonics for gauging and proximity sensing in air," J. Acoust. Soc. Am. 79, pp 1151-1160, 1986.
2. V. Magori and H. Walker, "Ultrasonic presence sensors with wide range and high resolution," IEEE Trans. Ultrasonics, Ferroelectrics, and Frequency Control, Vol. uffc-34, no. 2, pp. 202-210, 1987.
3. P. J. Westervelt, "Parametric end-fire array," J. Acoust. Soc. Am. 32, pp. 934-935(A), 1960; and

"Parametric acoustic array," J. Acoust. Soc. Am. 35, pp. 535-537, 1963.
4. M. B. Bennett and D. T. Blackstock, "Parametric array in air," J. Acoust. Soc. Am. 57, pp. 562-568, 1975.
5. N. S. Bakhalov, Ya. M. Zhileikin, and E. A. Zabolotskaya, Nonlinear Theory of Sound Beams, American Institute of Physics, New York, 1987.
6. V. P. Kuznetsov, "Equations of nonlinear acoustics," Sov. Phys. Acoust. 16, pp. 467-470, 1971.
7. L. E. Kinsler and A. R. Frey, Fundamentals of Acoustics, 2nd ed., John Wiley and Sons, New York, 1962.
8. G. S. Garrett, J. Naze Tjotta and S. Tjotta, "Nearfield of a large acoustic transducer. Part II: Parametric radiation," J. Acoust. Soc. Am. 74, pp. 1013-1020, 1983.
9. G. S. Garrett, J. Naze Tjotta, and S. Tjotta, "Nearfield of a large acoustic transducer. Part III: General results," J. Acoust. Soc. Am. 75, pp. 769-779, 1984.
10. J. Berntsen, J. Naze Tjotta, and S. Tjotta, "Nearfield of a large acoustic transducer. Part IV: Second harmonic and sum frequency radiation," J. Acoust. Soc. Am. 75, pp. 1383-1391, 1984.
11. F. H. Fenlon, and F. S. Mckendree, "Axisymmetric parametric radiation - A weak interaction model," J. Acoust. Soc. Am. 66, pp. 534-547, 1979.
12. M. F. Hamilton and F. H. Fenlon, "Parametric acoustic array formation in dispersive fluids," J. Acoust. Soc. Am. 76, pp. 1474-1492, 1984.
13. S. I. Aanonsen, T. Barkve, J. Naze Tjotta, and S. Tjotta, "Distortion and harmonic generation in the nearfield of a finite amplitude sound beam," J. Acoust. Soc. Am. 75, pp. 749-768, 1984.
14. M. F. Hamilton, J. Naze Tjotta, and S. Tjotta, "Nonlinear effects in the farfield of a directive sound source," J. Acoust. Soc. Am. 78, pp. 202-216, 1985.
15. S. I. Aanonsen, "Numerical computation of the nearfield of a finite amplitude sound beam," Rep. No. 73, Department of Mathematics, University of Bergen, Bergen, Norway, 1983.